Graphite Coating of Iron Nanowires for Nanorobotic Applications: Synthesis, Characterization and Magnetic Wireless Manipulation

Muhammad A. Zeeshan, Salvador Pané, Seul Ki Youn, Eva Pellicer, Simone Schuerle, Jordi Sort, Stefano Fusco, André M. Lindo, Hyung Gyu Park, and Bradley J. Nelson*

Wireless-manipulated graphite coated nanomagnets are promising candidates for minimally invasive targeted drug delivery platforms. Iron nanowires coated with graphitic shells are synthesized by template-assisted deposition. The use of porous aluminum oxide templates enables both the batch production of nanowires by electrodeposition and their subsequent conformal encapsulation in graphite using chemical vapor deposition (CVD). High quality graphitic shells are obtained when CVD conditions are optimized using acetylene as carbon feedstock at 740 °C. Interestingly, the iron nanowires transform into iron carbide during the CVD process leading to changes in magnetic properties. The graphite coated iron nanowires are precisely manipulated against a water flow (0.1 mm/s) using a magnetic field of 350 Oe and a gradient of 50 kOe m^{-1} in a 5-DOF magnetic manipulation system. Our approach opens new avenues for the design and synthesis of functional graphite coated nanowires that are promising for nanorobotics applications.

1. Introduction

Research on nanodevices for targeted drug delivery (TDD) applications has been pursued by scientists with the aim of overcoming the disadvantages associated with conventional therapies.[1] Materials science, pharmacy, engineering and other disciplines have contributed synergistically to the development of nanoscale TDD platforms in several aspects such as nanomaterials synthesis, nanofabrication, motion control, functionalization, drug dosing and triggering methods. A promising approach involves using magnetic nanoagents that can be wirelessly maneuvered by applying external magnetic fields.[2–7] This drug targeting strategy could reach confined spaces in the human body to locally deliver therapeutic drugs or molecular vectors. Magnetic nanoparticles (NPs) are the most common nanostructure used for biomedical applications such as magnetic resonance imaging (MRI), hyperthermia treatments or bioseparation.[2] However, if the magnetic nanostructure is used as an externally guided TDD platform, other geometries can be more advantageous. For instance, magnetic nanorods and nanowires (NWs) exhibit superior magnetic properties than NPs of comparable volume.[8,9] The high magnetic shape anisotropy of NWs results in their alignment along the long axis when applying external magnetic fields. In addition, high-aspect ratio nanostructures are taken up by cells more rapidly and efficiently than more isotropic geometries.[10]

A key issue concerning magnetic TDD systems is the functionalization of the nanostructure, and several efforts report on the direct functionalization of NW surfaces.[11] This approach, which can be attractive for biosensing or electronic applications, may be not suitable for TDD because the direct exposure of the magnetic NW surface to a biological environment can be cytotoxic. Moreover, the functionalization of magnetic NWs can be limited due to their surface chemistry or due to chemical degradation during the functionalization process. An attractive approach to incorporate functional moieties or molecular vectors onto the nanowires consists of coating the magnetic NWs with graphite layers. Carbonaceous nanomaterials such as graphene layers, single-walled (SWNT) and multi-walled (MWNT) carbon nanotubes can be functionalized using a wide range of chemical reactions.[12] The integration of carbonaceous coatings into magnetic TDD nanodevices allows the attachment of a wide variety of functional groups such as carboxylates, fluorines or amines, and the sp^2 hybridization of carbon enables functionalization via π–π interactions. Liu et al. have recently engineered nanoscale graphene oxide as a carrier for the

M. A. Zeeshan, Dr. S. Pané, S. Schuerle, S. Fusco, A. M. Lindo, Prof. B. J. Nelson
Institute of Robotics & Intelligent Systems (IRIS)
ETH Zürich, Zürich, Switzerland
E-mail: vidalp@ethz.ch
S. K. Youn, Prof. H. G. Park
Institute of Energy Technology
ETH Zürich, Zürich, Switzerland
Dr. E. Pellicer
Departament de Física
Facultat de Ciències
Universitat Autònoma de Barcelona
Bellaterra, Spain
Prof. J. Sort
Institució Catalana de Recerca i Estudis Avançats (ICREA), and Departament de Física
Universitat Autònoma de Barcelona
Bellaterra, Spain

DOI: 10.1002/adfm.201202046

delivery of an anticancer drug.[13] They also demonstrated wrapping SWNTs with polyethylene glycol (PEG) to reach tumor tissues in mice without apparent toxicity.[14] Yang et al. have demonstrated a dual drug delivery system based on a functionalized graphene oxide surface and iron oxide nanoparticles for targeted drug delivery.[15]

Several efforts propose the encapsulation of Fe NWs with carbon coatings for different applications such as magnetic nanosensors and magnetic recording media.[16–18] The saturation magnetization (M_S) of pure Fe is superior to that of most soft magnetic materials, while its biocompatible nature is also advantageous.[19–21] Therefore, it is an attractive element to be used in magnetic TDD nanodevices. Fe has extensively been used as an optimal catalyst to decompose carbon and produce CNTs.[19] The carbon coatings can be functionalized and act as a protective layer by preventing the development of antiferromagnetic oxide layers on the Fe. Thermolytic processes, such as pyrolysis, are the most common strategies to produce NW-filled carbonaceous cages.[22–25] However, these methods often lead to discontinuous filling,[26] irregular shapes,[27] and uneven distribution of material among the CNTs,[25] and, the use of metallocenes limits the filling material.

In the current work, we present a facile template-assisted batch synthesis of graphite-coated Fe NWs, their magnetic properties and magnetic manipulation of the NWs in a capillary tube. We demonstrate that Fe NWs are conformally coated by highly crystalline continuous graphitic shells under optimized conditions. The method uses anodic aluminum oxide (AAO) templates on silicon in which Fe NWs are produced by pulsed electrodeposition (PED) (see details on fabrication in the Supporting Information, S1 and S2).[5,6] Subsequently, the Fe NWs kept in the template are coated with graphite by chemical vapor deposition (CVD). Contrary to other methods, our approach allows the coating of the Fe NWs while still being embedded and aligned inside the pores of the template, which could be of interest for other applications such as magnetic recording or magnetic sensors.

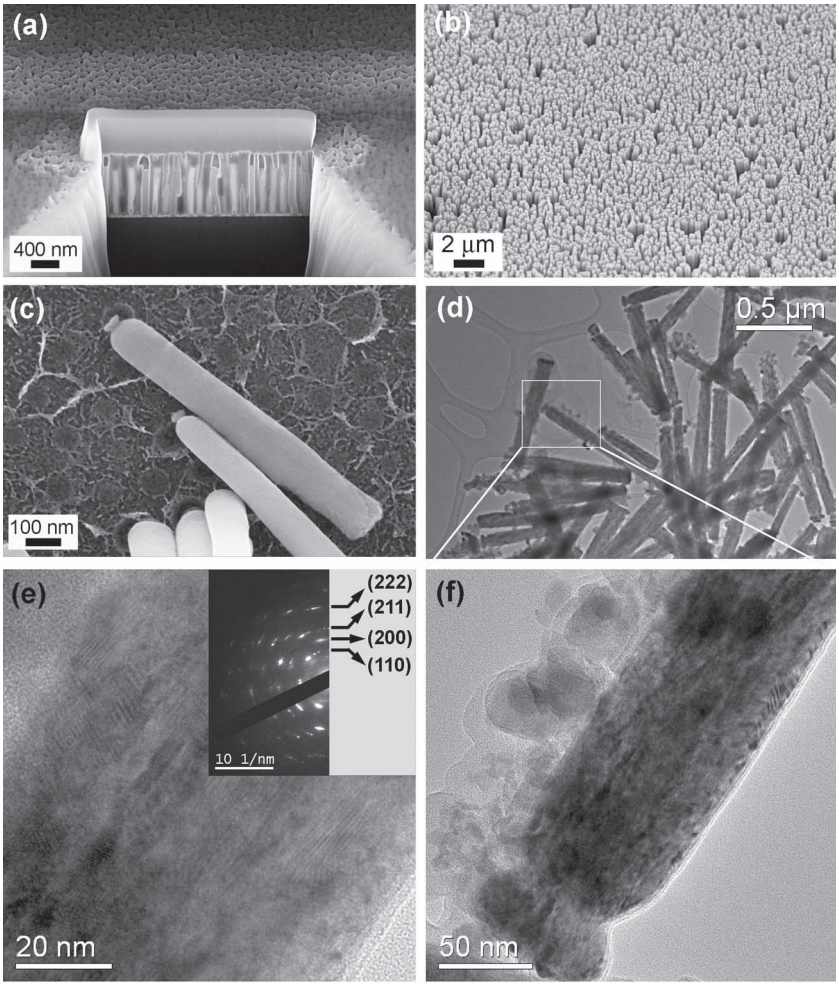

Figure 1. Characterization of electrodeposited Fe NWs: a) An FIB cross-section demonstrating uniform filling of AAO templates with Fe NWs. The cross-section was obtained after milling AAO templates with FIB at a milling current of 700 pA. A 1-µm-thick C protection layer was deposited with a inbuilt gas injection system (GIS) to avoid redeposition during milling. b) SEM image of an array of free-standing electroplated Fe NWs after the removal of AAO template with 10 wt% NaOH at 80 °C. c) SEM image of Fe NWs with a diameter of 115 nm and length of 1 µm. d) A bright field TEM image of as fabricated Fe NWs dispersed on a TEM grid, demonstrating length and diameter distribution. e) A HRTEM image of a single Fe NW featuring a moiré pattern confirming the polycrystalline nature of electrodeposited Fe. The inset shows the SAED pattern (the rings are compatible with bcc α-Fe). f) A HRTEM image of the base of the Fe NW enclosed in (d).

2. Results and Discussion

Fe NWs were synthesized by template assisted pulsed electrodeposition process (see the Experimental Section for details). **Figure 1**a shows a scanning electron microscopy (SEM) image of a cross-section made from a focused ion beam (FIB) at a milling current of 700 pA. The cross-section proves a uniform filling of the AAO template with Fe NWs. Figure 1b,c show typical SEM images of the Fe NWs after selective removal of the AAO template in NaOH at 80 °C. For transmission electron microscopy (TEM) and high-resolution TEM (HRTEM) observations (Figure 1d–f), a drop of NW suspension was deposited onto a TEM grid after 30 min sonication in methanol. HRTEM investigations in Figure 1e,f reveal a moiré pattern that clearly indicates the polycrystalline nature of the as deposited Fe NWs. This moiré pattern appears due to the overlapping of crystals with dissimilar orientations. The selected area electron diffraction (SAED) pattern shown in the inset of Figure 1e displays spotty rings whose interplanar distances match those expected for the α-Fe (bcc) phase. The X-ray diffraction (XRD) pattern of Fe NWs embedded inside the AAO template was also taken to

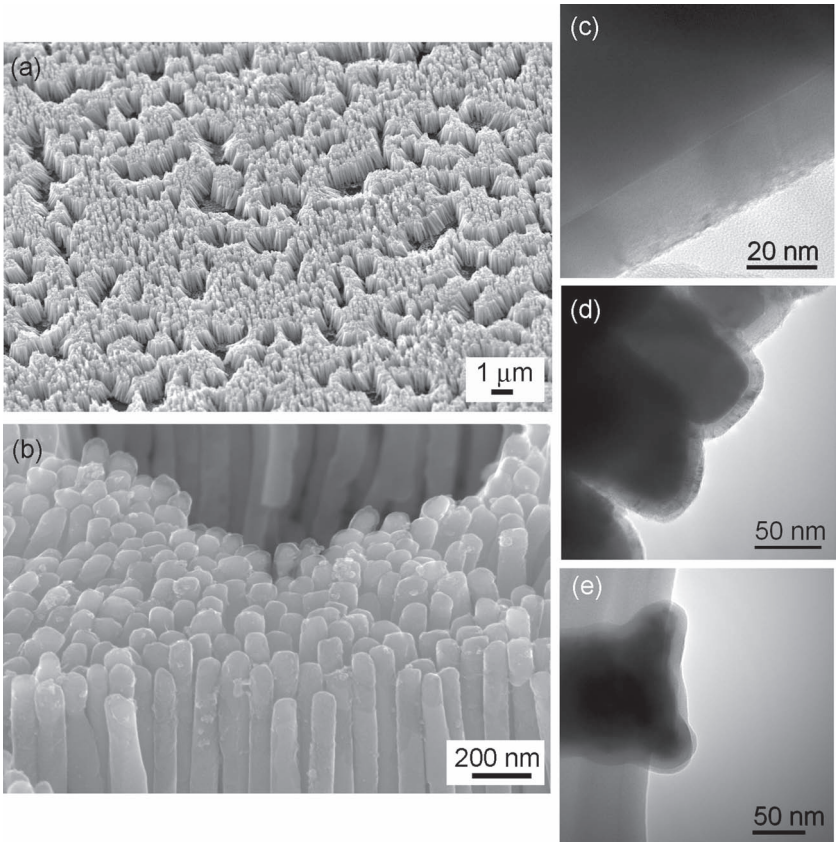

Figure 2. Electron micrographs of Fe NWs after CVD process: a) SEM image of a free-standing vertical array of graphite-coated Fe NWs obtained after removal of AAO template. b) A higher magnification SEM image showing the Fe NWs, featuring a brighter contrast, covered by the carbon shells, which look slightly darker. The length of these structures is in the range of 500 nm to 1.6 μm. c–e) Bright field TEM images demonstrating a high quality conformal graphitic coating covering all regions of the NWs including side, tip and base, respectively.

confirm the α-Fe (bcc) phase. An XRD pattern of as deposited NWs is provided in the Supporting Information (S3).

After the electrodeposition step, a CVD process was carried out in a controlled environment to coat Fe NWs with graphitic shells (see details in the Experimental Section). **Figure 2** shows SEM and TEM images that highlight the successful and uniform coverage of Fe NWs with graphitic shells. Images were taken after removing the AAO templates with NaOH as described earlier. A thick layer of carbon coats each NW, as shown in Figure 2b. A vertical array (Figure 2a) of these hybrid nanostructures allows the possibility of up scaling the process to a wafer size. In order to evaluate the quality of the carbon coatings, in-depth TEM analysis was carried out. Prior to TEM observations, a cleaning process was developed to remove the debris from the surface of the hybrid structures (see the Supporting Information, Figure S4), which is explained in detail in the Experimental Section. From Figure 2c–e, TEM observations reveal that the entire NW surface is conformally coated with graphitic shells including the sidewall, tip and base. The images confirm the effectiveness of the template-assisted CVD process. In Figure 2d, the shell thickness at the tips is 10–14 nm, although it may vary depending on the NW diameter. It is known that shell thickness is strongly dependent on the synthesis parameters and NW shape modifications are dependent on temperature and pressure of the chamber.[17,28]

Smooth and fully conformal coating by the graphitic layer of the curved NW cap and sidewall was obtained only within the growth time range of 3–5 min. This complete graphite coating at both ends and the side of each NW indicates that a typical base or tip growth mechanism of CNT growth cannot be a suitable model for our case.[29,30] For shorter growth times, incomplete coatings and structural deformation were observed. For growth times larger than 5 min, undesired formation of amorphous carbon on the underlying graphitic layers was obtained (see Supporting Information, S5). These observations indicate that the mechanism of graphene synthesis corresponding to a dissolution-precipitation process applies.[31–33] During the coating process, one could observe that Fe NWs deform their tip shape from a previously flat cap to a more hemispherical or elongated protrusion. Earlier, Rodriguez-Manzo et al. reported similar findings that such deformation occurs simultaneously or shortly after the nucleation of graphitic layer and can be attributed to the wetting effect by the graphene surface layer.[34] The optimal coating was observed with a modified hemispherical tip, indicating that the formation of hemispherical shape is crucial for nucleating graphitic shells. An elongated protrusion of the coated Fe NW was also observed, caused by the internal pressure build-up between the encapsulated NW and the graphitic shells leading to plastic deformation (see Supporting Information, S6).[35]

Aside from morphological changes, structural modifications of the core material were also observed after the CVD process (see **Figure 3**). Figure 3a displays a HRTEM image showing a conformal coating of graphitic shells around a tip of NW. The shell thickness at this region is 20.5 nm with an interlayer spacing of 3.38 Å (approximately 60 shells), which matches the (002) plane of graphite carbon. The intensity profile of the graphitic shell structure is given in Figure 3b, and a high-resolution TEM image of the NW-graphite interface is shown in Figure 3c. From the corresponding SAED (Figure 3d) and XRD (Figure 3e) patterns, the presence of the cementite phase (Fe_3C) was revealed, suggesting that α-Fe was converted to Fe_3C during the CVD process. The interface between the graphitic shells and the Fe_3C core disclosed by the HRTEM images clearly show that the plane fringes of the Fe_3C are not parallel to the (002) fringes of graphite (see Figure 3c).

To further explore the crystallinity of graphitic surfaces, the Raman spectrum of carbon-coated Fe NWs was obtained after the removal of the AAO template. Because it is relatively difficult to acquire the spectrum of an individual NW due to their high density, the analysis was made at various locations

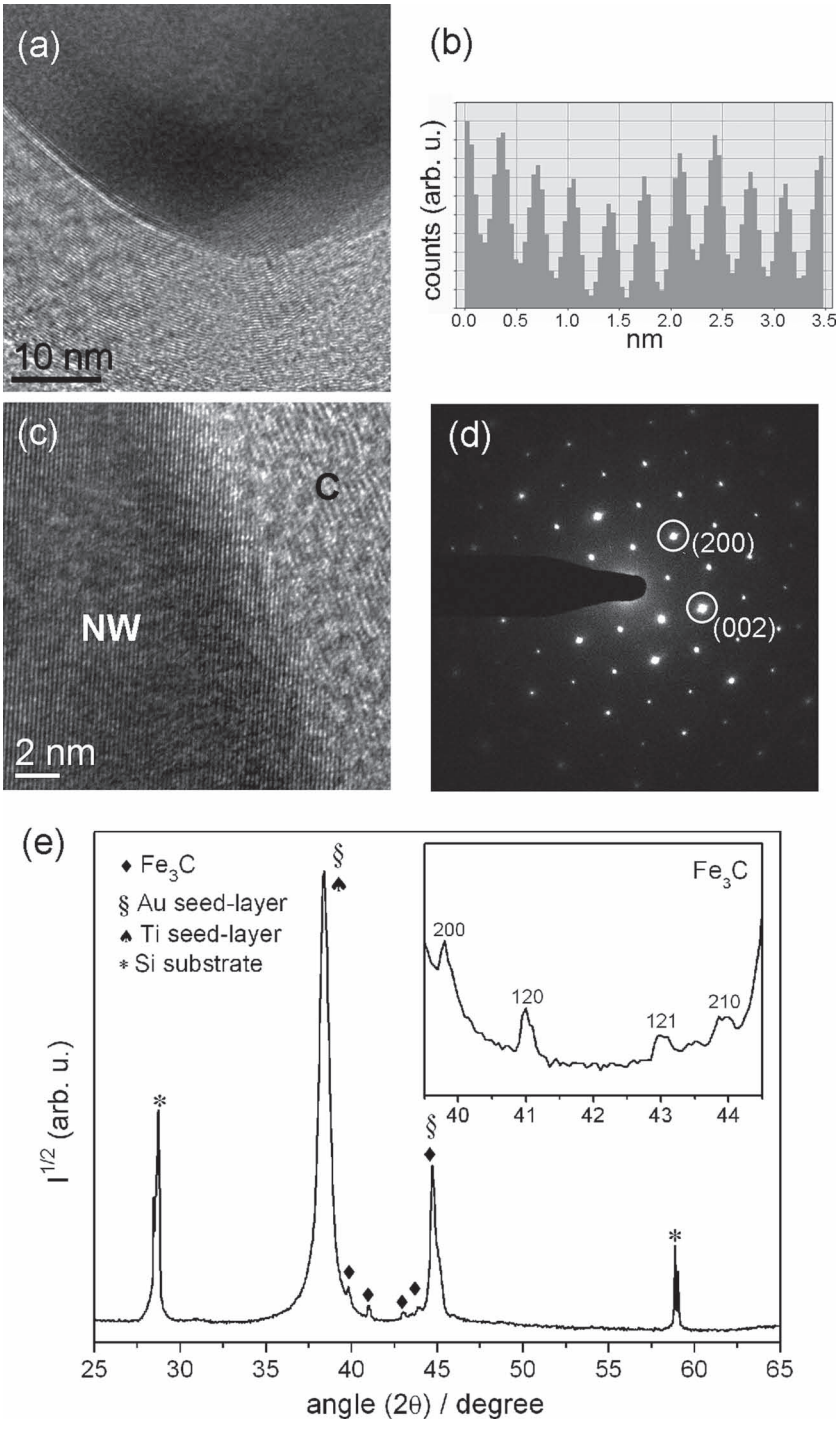

Figure 3. a) HRTEM image of a Fe NW conformally coated with high quality graphitic shells with an overall thickness of around 20.5 nm. The interlayer spacing between the shells is 3.38 Å with approximately 60 shells. b) Intensity profile of the shell structure. c) HRTEM image taken at the NW-graphite interface. The lattice fringes of the dark region (NW) correspond well with a (001) plane of cementite (Fe_3C) phase ($d = 2$ Å). d) Selected area electron diffraction (SAED) pattern of the NW core. The spots match with the cementite phase. e) XRD pattern of graphite-coated Fe NWs embedded in a AAO template confirming the presence of the cementite phase after the CVD process. The inset shows a detailed profile within the 39.5°–44.5° 2θ region.

across the chip to obtain an overall estimate of the degree of graphitization. The Raman spectrum of mechanically stripped graphite was also taken for comparison. In the Raman spectra of **Figure 4**, the first order characteristic G band, inherent in all sp^2 carbon allotropes and attributed to in-plane stretching of C–C bonds,[36,37] is found at a Raman shift of 1582 cm^{-1}. On the other hand, the second order vibration G′(2D) band is located around 2610 cm^{-1}. The small G′-to-G ratio is characteristic to multiple graphitic layers.[38] Both G and G′ bands confirm the high degree of graphitization of the carbon shells that coat the electrodeposited Fe NWs. In addition to these bands, a D-band peak was observed around 1330 cm^{-1} indicating existence of some defects on the graphitic surfaces commonly produced during CVD synthesis.[39]

The magnetic characterization of our graphite coated Fe NW samples was carried out by vibrating sample magnetometry (VSM). **Figure 5** shows the hysteresis loops of the arrays of NWs embedded in the AAO templates, both before and after the CVD coating, measured parallel (∥) and perpendicular (⊥) to the NW axis directions. Due to the shape anisotropy, an isolated NW with a large aspect ratio should exhibit a square hysteresis loop when the magnetic field is applied parallel to the NW axis and a tilted hard-axis loop along the ⊥ direction.[40,41] Conversely, the investigated arrays of NWs exhibit sheared hysteresis loops along both directions of measurement with rather low values of coercivity, H_C, and remanence-to-saturation magnetization ratio, M_R/M_S. Remarkably, the slope of the central part of the loops is even lower along the ∥ direction, thus suggesting that the magnetic easy axis is perpendicular to the NW axis. Such an observation can be ascribed to the competition between shape anisotropy, magnetocrystalline anisotropy and the dipolar fields created between neighboring NWs.

For a two-dimensional infinite array of cylindrical particles with radius r, length L, aspect ratio $A_r = L/2r$ and interwire distance D, the total dipolar field when all NWs are oriented along the ∥ direction can be written as:[42–44]

$$H_{\mathrm{dip},0^\circ} = \frac{4.2 M_S \pi r^2 L}{D^3} \quad (1)$$

If all moments are aligned perpendicular to the NW direction, then the dipolar field would be:

$$H_{\mathrm{dip},90^\circ} = \frac{-2.1 M_S \pi r^2 L}{D^3} \quad (2)$$

In turn, the demagnetizing field of one NW can be expressed as:

$$H_{\mathrm{demag}} = (N_\perp - N_{||}) M_S \quad (3)$$

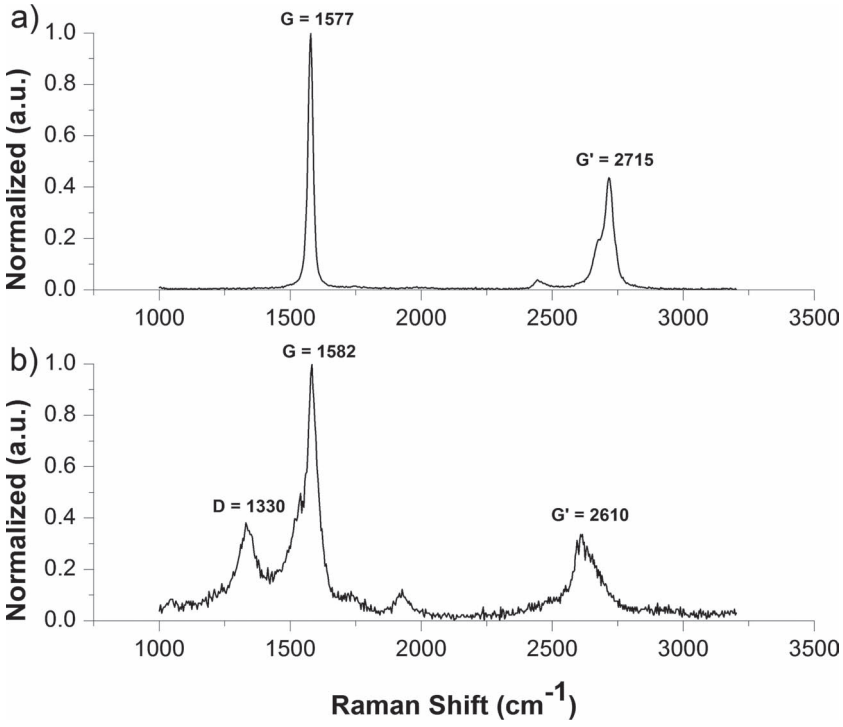

Figure 4. a) Raman spectrum of mechanically stripped graphite (HOPG) with G and G′ bands at 1577 and 2715 cm^{-1}, respectively. b) Raman spectrum from an array of graphite-coated Fe NWs with normalized G band at 1582 cm^{-1}. The D band is observed at a Raman shift of 1330 cm^{-1}, whereas the G′ band appeared at 2610 cm^{-1}. G and G′ bands clearly signify sp^2 characteristic graphitic surface coatings.

where $N_{\parallel}$ and $N_{\perp}$ are the demagnetizing factors along the NW axis and its perpendicular direction respectively, and can be calculated using a prolate spheroid approximation as:[45]

$$N_{\parallel} = \frac{4\pi}{A_r^2 - 1}\left[\frac{A_r}{2\sqrt{(A_r^2-1)}}\ln\left(A_r + \sqrt{A_r^2 - 1}\right) - 1\right] \quad (4)$$

$$N_{\perp} = \frac{4\pi - N_{\parallel}}{2} \quad (5)$$

The total effective anisotropy field can then be expressed as:

$$H_{K,\text{eff}} = (N_{\perp} - N_{\parallel})M_S - \frac{6.3\,M_S \pi r^2 L}{D^3} + H_{mc} \quad (6)$$

H_{mc} is the magnetocrystalline anisotropy contribution which, to a first approximation, can be neglected given the relatively low intrinsic value of magnetocrystalline anisotropy for cubic α-Fe and the averaging effect from the polycrystalline character of the NWs (Figure 1e,f), which further reduces H_{mc}.

Equation 6 predicts that if $H_{K,\text{eff}}$ is negative, the magnetic easy axis will be perpendicular to the NW axis; otherwise, for positive $H_{K,\text{eff}}$ values, the magnetic easy axis will be parallel (||).[43] Assuming that $r \approx 50$ nm and $L \approx 700$ nm, Equation (4) and (5) give: $N_{\perp} = 6.239 \approx 2\pi$ and $N_{\parallel} = 0.086 \approx 0$. Then, considering that the average distance between two neighboring NWs is around 150 nm (see Figure S1, Supporting Information), Equation 6 shows that $H_{K,\text{eff}} < 0$, thus accounting for the observed lower shearing of the loop measured along the direction, i.e., along the substrate plane direction (Figure 5). This crossover of the magnetic easy axis occurs mainly because of the proximity between NWs. In the limiting case when all the NWs would be in direct contact with each other, the situation reminiscent of a continuous thin film, where shape anisotropy dictates magnetic easy axis along the film plane. Strictly speaking, Equations (1) and (2) are valid only for ordered square arrays of cylindrical dots.[42] In our case, the NWs are arranged randomly inside the pores of the AAO templates. However, it has been shown that such geometrical disorder tends to induce further shearing of the hysteresis loops and an increase of the saturation field.[47]

The post CVD magnetic measurements reveal that the saturation magnetization decreases by a factor of almost 2, while the coercivity increases. This is not surprising, bearing in mind that the value of M_S in Fe_3C is roughly half that of α-Fe.[47] In turn, the coercivity along the direction increases from 250 Oe to 310 Oe after coating. This increase is due to the magnetically harder

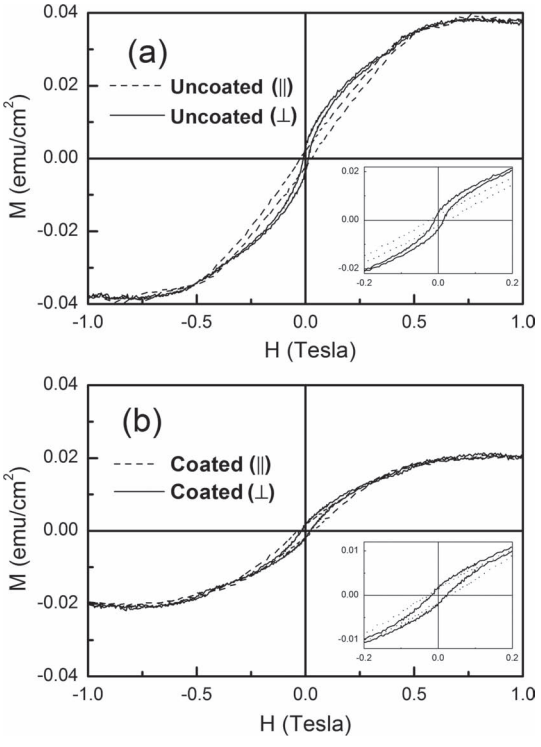

Figure 5. Hysteresis loops, measured at room temperature, corresponding to the arrays of (a) the uncoated Fe NWs and (b) the NW after the CVD coating, both parallel (||) and perpendicular (⊥) to the NW axis. Note that magnetization (M) is normalized by the measured overall area of the AAO template.

character of Fe_3C as compared to soft α-Fe. Also, since the crystallite size tends to increase during the CVD, the averaging effect in H_{mc} is reduced and the net magnetocrystalline anisotropy is enhanced, thus causing an increase of H_C. The dipolar interactions between the NWs have also a strong influence in H_C and M_R/M_S, therefore, reducing both parameters significantly with respect to the values in isolated non-interacting NWs.[48,49] Finally, magnetic curling and buckling effects cannot be completely ruled out since the diameter of the Fe NWs is relatively large. Such inhomogeneous magnetization reversal modes would also tend to reduce H_C, as compared to coherent rotation of single-domain states.

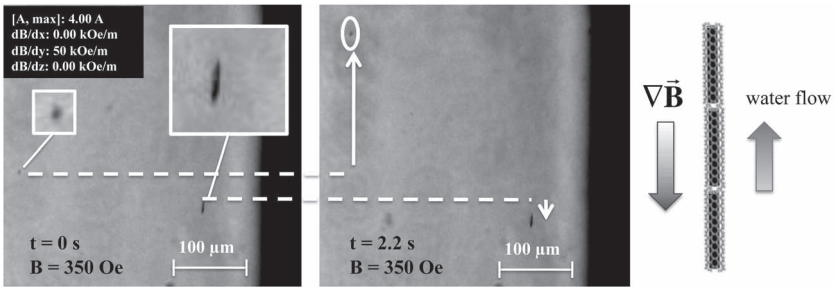

Figure 6. A manipulation sequence of a graphite coated Fe NW agglomerate with a length of around 15 µm being held against the flow in a glass capillary (diameter of 580 µm). The flow rate is 0.1 mm/s when a constant field of 350 Oe was applied in the positive *y*-direction. A magnetic gradient of 50 kOe/m was applied in negative *y* direction against the direction of flow in order to hold the agglomerate against the flow.

To wirelessly manipulate graphite coated Fe NWs, a glass capillary with a diameter of 580 µm, in the range of a human capillary, was connected to a fluidic system and fixed in a custom-made holder above the objective. Manipulation experiments were conducted in a specially designed 5-DOF system equipped with 8 electromagnetic coils (details on the manipulation system can be found in the Experimental Section).[50] A flow rate of 0.1 mm s^{-1} was set and confirmed by the flow velocity of nonmagnetic reference particles (polysterene beads, Polyscience), 6 µm in diameter, that were injected into the feeding pipe at a location approximately 20 cm ahead of the glass capillary. We assume a fully developed laminar flow obeying Hagen-Poiseuille law and hence, a parabolic flow profile. To confirm the flow rate, the translational distance was measured for particles passing the center of the glass channel, particles at the maximum velocity. The graphite-coated Fe NW solution had a concentration of approximately 1 mg mL^{-1} and 1 mL of the solution was injected into the flow system at the same position as the reference particles. First a rotating magnetic field at 350 Oe and 0.2 Hz was applied in order to detect when the graphite-coated NWs reached the glass capillary. A constant field of 350 Oe was then applied in the positive *y*-direction, which aligned the long axis of the graphite-coated NWs with the capillary's axis. A magnetic gradient of 50 kOe m^{-1} was applied in negative *y* against the flow direction.

Figure 6 shows a sequence where a 15-µm-long agglomerate of several aligned single graphite-coated Fe NWs was pulled against the flow at the given applied magnetic field and gradient magnitude. The resulting velocity of the graphite-coated NWs is defined by the sum of the velocity induced by the magnetic force and by the hydrodynamic force. Within 2.2 s, a reference bead moved approximately 180 µm corresponding to a flow rate of 0.08 mm s^{-1}. The graphite-coated NW bundle was pulled in the opposite flow direction by approximately one body length within the same time frame. A magnetic field of 350 Oe and a field gradient of 50 kOe m^{-1} was applied. Other manipulation sequences in a static flow are shown in the Supporting Information (Figure S7).

Although the applied magnetic field for the manipulation (350 Oe) is low compared to the saturation field from the hysteresis loops shown in Figure 5 (H_{sat} > 7000 Oe), this external field is larger than H_C and is sufficient to align, accelerate and decelerate the NWs. Once the NWs are removed from the AAO templates, dipolar interactions are no longer present and the hysteresis loops would then become rather square along the NW axis due to shape anisotropy. This explains why the NWs orient parallel and not perpendicular to the external field during manipulation and why they can be maneuvered despite the apparently low magnetization value that, according to Figure 5, would correspond to H = 350 Oe.

As a proof of concept, preliminary experiments regarding the functionalization of the magnetic graphite-coated NWs were realized according to the protocol of Liu et al.[14] Provided that the graphitization level of the carbon coatings is high, a noncovalent functionalization of conjugated aromatic molecules through supramolecular π–π stacking is considered.[53] Noncovalent functionalization of carbonaceous nanostructures is an advantageous approach respect to the covalent one.[14] The covalent attachment usually implies degradation of the carbon shells and the harsh chemical conditions employed might also lead to partial or total etching of the inner magnetic core. Advantageously, the noncovalent functionalization proposed preserves the intrinsic optical properties of the carbonaceous nanostructures,[14] which makes the graphite-coated NWs a great tool for biological applications such as imaging and sensing. **Figure 7**a shows schematically the conjugation of Rhodamine B (Rh-B), a molecule used as a hydrophobic model drug, on the phospholipid-polyethyleneglycol (PL-PEG) functionalized carbonaceous nanomagnets. PL-PEG acts as a linker for the attachment of biomolecules and also provides water solubility which is important for biomedical applications. Figure 7b shows the UV-vis absorption spectra for PL-PEG functionalized graphite-coated NWs and the PL-PEG functionalized graphite-coated NWs loaded with Rh-B (absorption peak at 554 nm). The spectrum corresponding to the remaining level of Rh-B in solution is also shown as a control and compared with the water spectrum. In order to confirm that Rh-B was attached to the carbonaceous nanomagnets, a similar test was run in a medium without the graphite-coated NWs. In this case, small amount of Rh-B was detected, thus confirming that most of the Rh-B present in the medium containing the graphite-coated NWs was effectively anchored to the carbon shells.

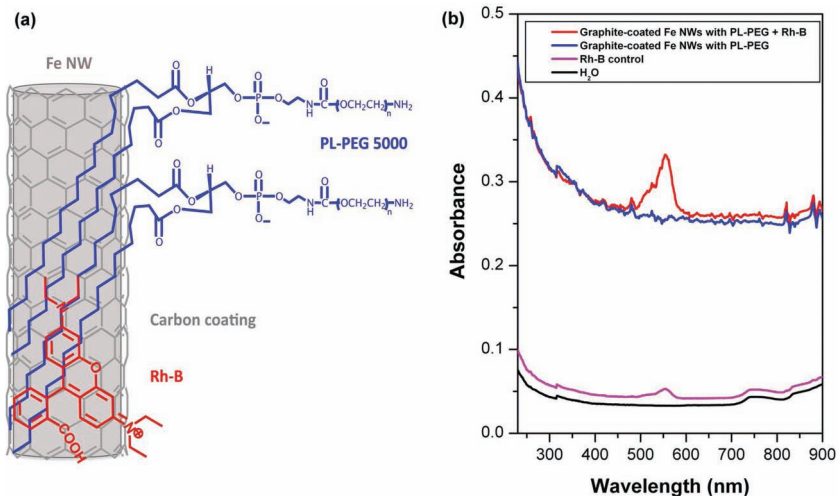

Figure 7. a) Scheme showing the functionalization of graphite-coated Fe NWs with Rh-B using PL-PEG 5000. b) UV-vis absorbance spectra of solutions of graphite-coated Fe NWs functionalized with PL-PEG (blue), graphite coated Fe NWs functionalized with PL-PEG + Rh-B (red), remaining free Rh-B after following the protocol without the graphitic nanostructures (magenta) and DI-water (black).

3. Conclusions

We have successfully demonstrated a facile approach to conformally coat Fe NWs with high quality graphitic layers using a template-assisted CVD technique. SEM, TEM, XRD, and Raman spectroscopy were used to evaluate the uncoated and coated NWs. Characterization of the magnetic properties showed that graphite coated NWs exhibit lower M_S than uncoated NWs due to the transformation of α-Fe to Fe_3C. Controlled manipulation of the coated NWs using a 5-DOF magnetic manipulation system has been demonstrated. The results show that the template-assisted CVD technique is an efficient approach to manufacture in batch magnetic targeted drug delivery platforms.

4. Experimental Section

Preparation of Anodic Aluminum Oxide Templates: Anodic aluminum oxide (AAO) templates with a uniform and parallel porous structure were prepared by anodizing an e-beam evaporated layer of Al (1.5–2 µm thick) on Si substrate with Ti and Au-seed layers as reported previously.[5,6] A current controlled single-step anodization was carried out in 0.3 M oxalic acid. A lead electrode was used as the counter electrode and a potential of 60 V was applied to obtain AAO templates. The temperature inside the anodizing bath was maintained at 5 °C using a cryostat. After anodization, a pore widening treatment was conducted in a 5 wt% phosphoric acid to decrease the barrier layer and increase the diameter of the templates (Figure S1.1, Supporting Information). ImageJ, a public domain image-processing tool, was used to estimate the pore size and the pore distribution. A feret diameter distribution of 103 ± 11 nm was obtained after SEM image analysis (Figure S1.2, Supporting Information).

Electrodeposition of Fe NWs: Fe NWs were uniformly electrodeposited into the pores of the AAO template by using pulsed electrodeposition (PED) (Table S2.2, Supporting Information). All the depositions were carried out at room temperature (25 °C) with a constant stirring rate of 200 rpm. The counter electrode for electrodeposition was a platinized Ti sheet with dimensions of 10 cm × 10 cm. N_2 bubbling was maintained during all depositions in order to avoid oxidation. The length of the NWs was controlled by fixing the charge density, q, and all the depositions of Fe NWs were carried out at a constant current density, j, of –125 mA cm^{-2}. A newly designed electrolyte was used for electroplating Fe NWs which is described in the Supporting Information S2.

Chemical Vapor Deposition Process for Graphitic Coatings Around NWs: For synthesizing graphite coated Fe NWs, a chemical vapor deposition (CVD) process was utilized. AAO templates filled with electrodeposited Fe NWs were placed on a graphite heater inside a commercial low pressure CVD system (Aixtron Ltd, Black Magic) equipped with a shower gas system, which allowed a precise laminar gas flow with a uniform supply of gases, high carbon efficiency and uniform growth over larger areas.[51] The target temperature, temperature ramp, pressure and flow rates were controlled by the software interface. The heating was provided by a heated graphite stage and the temperature was controlled with an infrared temperature sensor. The temperature was ramped at 300 °C min^{-1} up to the annealing temperature of 710 °C with a H_2/Ar flow of 200 and 300 sccm, respectively. For the growth temperature stabilization and additional reduction, the chamber was maintained at 740 °C for 5 min before adding C_2H_2 into the chamber. The desired temperature was achieved and stabilized after approximately 120 s. The growth time was varied between 45 s and 10 min and the total pressure, P_T, was fixed at 3 mbar with a C_2H_2 partial pressure of 0.025 mbar. The partial pressure ratio of C_2H_2 to H_2 was maintained at 1:40. After growth the CVD chamber was cooled in an Ar environment at approximately 22 °C min^{-1} and samples were removed at a temperature below 400 °C.

Cleaning Process: Free-standing uncoated and coated Fe NWs were obtained after removal of the AAO template using 10 wt% NaOH solution at 80 °C for 5 min. The resulting arrays were then rinsed successively with 95% ethanol in order to avoid reprecipitation of alumina, as reported by Magnin et al.[52] Coated and uncoated NWs were collected in methanol by sonicating the chips at 40 kHz for 1 h. To remove the traces of NaOH, a neutralization step was carried out in 1 wt% citric acid for 5 min. Finally, uncoated and coated NWs were centrifuged (14 000 rpm, 10 min), and the supernatant was decanted and replaced with absolute ethanol a minimum of five times.

Characterization Techniques: The morphology of the samples was characterized using a field emission scanning electron microscope (FESEM, Zeiss NVision 40) equipped with focused ion beam (FIB). Prior to imaging with a transmission electron microscope (TEM, Philips CM12, 100 kV) and a high-resolution transmission electron microscope (HRTEM, FEI Tecnai F30, 300 kV), coated and uncoated Fe NWs were dispersed on an ultrathin carbon film on holey carbon support film, 400 mesh (Pelco, 01824). X-ray diffraction (XRD) patterns were taken while keeping the coated and uncoated NWs inside the AAO template (Cu Kα radiation).

Raman Spectroscopy: A WITec CRM200 spectrometer equipped with a 532 nm green laser was used to record the Raman spectra at room temperature. The spectra of coated Fe NWs were obtained after removing the AAO template.

Magnetic Characterization: Both coated and uncoated Fe NWs embedded in AAO templates were mounted inside vibratory sample magnetomery (VSM, Oxford Instruments 1.2). Magnetic hysteresis loops were obtained at room temperatures by applying magnetic field of 1 T.

Magnetic Manipulation: Manipulation experiments were conducted with a specially designed 5-DOF magnetic manipulation system based on eight electromagnets. The system is capable of producing magnetic fields as high as 500 Oe and gradients up to 50 kOe m^{-1}.[50] For optical tracking of nanoagents the system is integrated with an inverted fluorescence microscope (Olympus IX 81). The set of electromagnets is arranged in a single hemisphere and the sample is placed between

the coil arrangement and the objective. In the experiments, parameters such as magnetic field strength and the field gradients were controlled by the user. A maximum-filed strength of 350 Oe was generated in the positive y direction. A gradient of 50 KOe/m was applied in the opposite y direction opposite to the direction of the flow. In the experiments, the magnetic field was applied along the long axis of the graphite coated Fe NWs. A video of the manipulation experiment is provided in the Supporting Information.

Functionalization: Graphite-coated NWs were functionalized with PL-PEG5000-amine (1:5 mass ratio (CNT:PL-PEG)) by dissolution in water (5 mL) into a 20 mL-glass scintillation vial. The vial was sonicated for 1 h at room temperature. Water was changed periodically to avoid overheating. The nanocapsules suspension were centrifuged at 14 500 rpm for 3 h at room temperature and the supernatant solution was then collected. The PL-PEG functionalized nanocapsules suspension was placed into a 0.5 mL-Amicon centrifugal filter device with a molecular weight cutoff (MWCO) of 100 kDa. The filter device was filled with water to the limit and the solution was centrifuged at 14 500 rpm for 10 min at room temperature. The excess of PL-PEG in the nanocapsule suspension was removed by successive washings/centrifugation cycles. Afterwards, PL-PEG5000-Amine-functionalized nanocapsules (0.5 mL) were mixed with Rh-B (30 µL, 1 mM) solution and water (50 µL) was added. The mixture was stored at 4 °C for 24 h. The excess of Rh-B was then removed using the Amicon centrifugal filter device and subsequently washed/centrifuged 10 times using water. After intensive filtration the Rh-B functionalized nanocapsules retained a slight pink color. The functionalized nanocapsules were finally resuspended in water (0.5 mL) and centrifuged at 14 500 rpm for 10 min at 4 °C to remove aggregates.

Supporting Information

Supporting Information is available from the Wiley Online Library or from the author.

Acknowledgements

The authors would like to thank Dr. Fabian Gramm of the Electron Microscopy Center (EMEZ) of ETH Zürich for his help on HRTEM analysis. We would also like to thank Susan Droescher for providing mechanically stripped graphite for Raman comparisons. We thank the FIRST laboratory for their technical support. Funding for this research was provided by the project "Nano-Actuators and Nano-Sensors for Medical Applications (NANOMA)" funded by the European Commission under the Seventh Framework Program (FP7). E.P. and J.S. acknowledge financial support from the Spanish Ministry of Economy and Competitivity (project MAT2011-27380-C02-01).

Received: July 23, 2012
Published online: September 21, 2012

[1] B. P.Timko, T. Dvir, D. S. Kohane, *Adv. Mater.* **2010**, *22*, 4925.
[2] E. Ruiz-Hernández, A. Baeza, M. Vallet-Regí, *ACS Nano* **2011**, 1259.
[3] V. K. Varadan, L. Chen, J. Xie, *Nanomedicine: Design and Applications of Magnetic Nanomaterials, Nanosensors and Nanosystems*, John Wiley & Sons, Ltd: **2008**; pp 129–173.
[4] L. Clime, B. Le Drogoff, S. Zhao, Z. Zhang, T. Veres, *Int. J. Nanotechnol.* **2008**, *5*, 1268.
[5] M. A. Zeeshan, K. Shou, S. Pané, E. Pellicer, J. Sort, K. M. Sivaraman, M. D. Baró, B. J. Nelson, *Nanotechnology* **2011**, *22*, 275713.
[6] M. A. Zeeshan, K. Shou, K. M. Sivaraman, T. Wuhrmann, S. Pané, E. Pellicer, B. J. Nelson, *Mater. Today* **2011**, *14*, 54.
[7] L. Zhang, T. Petit, Y. Lu, B. E. Kratochvil, K. E. Peyer, R. Pei, J. Lou, B. J. Nelson, *ACS Nano* **2010**, *4*, 6228.
[8] A. Hultgren, M. Tanase, E. J. Felton, K. Bhadriraju, A. K. Salem, C. S. Chen, D. J. Reich, *Biotechnol. Prog.* **2005**, *21*, 509.
[9] M. Safi, M. Yan, M.-A. Guedeau-Boudeville, H. Conjeaud, V. Garnier-Thibaud, N. Boggetto, A. Baeza-Squiban, F. Niedergang, D. Averbeck, J.-F. Berret, *ACS Nano* **2011**, *5*, 5354.
[10] S. E. A. Gratton, P. A. Ropp, P. D. Pohlhaus, J. C. Luft, V. J. Madden, M. E. Napier, DeSimone, *Proc. Natl. Acad. Sci. USA* **2008**, *105*, 11613.
[11] J. Wang, *ChemPhysChem* **2009**, *10*, 1748.
[12] Y.-P. Sun, K. Fu, Y. Lin, W. Huang, *Acc. Chem. Res.* **2002**, *35*, 1096.
[13] Z. Liu, J. T. Robinson, S. M. Tabakman, K. Yang, H. Dai, *Mater. Today* **2011**, *14*, 316.
[14] Z. Liu, S. M. Tabakman, Z. Chen, H. Dai, *Nat. Protoc.* **2009**, *4*, 1372.
[15] X. Yang, Y. Wang, X. Huang, Y. Ma, Y. Huang, R. Yang, H. Duan, Y. Chen, *J. Mater. Chem.* **2011**, *21*, 3448.
[16] V. V. Ivanovskaya, C. Köhler, G. Seifert, *Phys. Rev. B* **2007**, *75*, 075410.
[17] A. Leonhardt, S. Hampel, C. Müller, I. Mönch, R. Koseva, M. Ritschel, D. Elefant, K. Biedermann, B. Büchner, *Chem. Vap. Deposition* **2006**, *12*, 380.
[18] A. Winkler, T. Muhl, S. Menzel, R. Kozhuharova-Koseva, S. Hampel, A. Leonhardt, B. Büchner, *J. Appl. Phys.* **2006**, *99*, 104905.
[19] D. L. Huber, *Small* **2005**, *1*, 482.
[20] L. Chen, J. Xie, K. R. Aatre, V. K. Varadan, *J. Nanotechnol. Eng. Med.* **2010**, *1*, 011009.
[21] M.-M. Song, W.-J. Song, H. Bi, J. Wang, W.-L. J. Sun, M. Yu, *Biomaterials* **2010**, *31*, 1509.
[22] W. Wang, K. Wang, R. Lv, J. Wei, X. Zhang, F. Kang, J. Chang, Q. Shu, Y. Wang, D. Wu, *Carbon* **2007**, *45*, 1127.
[23] S. Hampel, A. Leonhardt, D. Selbmann, K. Biedermann, D. Elefant, C. Muller, T. Gemming, B. Buchner, *Carbon* **2006**, *44*, 2316.
[24] R. T. Lv, F. Y. Kang, W. X. Wang, J. Q. Wei, X. F. Zhang, Z. H. Huang, J. L. Gu, K. L. Wang, D. H. Wu, *Phys. Status Solidi A.* **2007**, *204*, 867.
[25] R. Sen, A. Govindaraj, C. N. R. Rao, *Chem. Phys. Lett.* **1997**, *267*, 276.
[26] N. S. Kim, Y. T. Lee, J. Park, J. B. Han, Y. S. Choi, S. Y. Choi, J. Choo, G. H. Lee, *J. Phys. Chem. B* **2003**, *107*, 9249.
[27] N. Grobert, M. Mayne, M. Terrones, J. Sloan, R. E. Dunin-Borkowski, R. Kamalakaran, T. Seeger, H. Terrones, M. Ruhle, D. R. M. Walton, H. W. Kroto, J. L. Hutchison, *Chem. Commun.* **2001**, 471.
[28] N. Bajwa, X. Li, P. M. Ajayan, R. Vajtai, *J. Nanosci. Nanotechnol.* **2008**, *8*, 6054.
[29] M. Kumar, Y. Ando, *J. Nanosci. Nanotechnol.* **2010**, *10*, 3739.
[30] K. J. MacKenzie, O. M. Dunens, A. T. Harris, *Ind. Eng. Chem. Res.* **2010**, *49*, 5323.
[31] Y. G. Yao, Z. Li, Z. Y. Lin, K. S. Moon, J. Agar, C. P. Wong, *J. Phys. Chem. C* **2011**, *115*, 5232.
[32] R. T. K. Baker, D. J. C. Yates, J. A. Dumesic, *ACS Symp. Ser.* **1983**, *202*, 1.
[33] R. T. K. Baker, P. S. Harris, R. B. Thomas, R. J. Waite, *J. Catal.* **1973**, *30*, 86.
[34] J. A. Rodríguez-Manzo, M. Terrones, H. Terrones, H. W. Kroto, L. T. Sun, F. Banhart, *Nat. Nanotechnol.* **2007**, *2*, 307.
[35] L. Sun, F. Banhart, A. V. Krasheninnikov, J. A. Rodríguez-Manzo, M. Terrones, P. M. Ajayan, *Science* **2006**, *312*, 1199.
[36] M. S. Dresselhaus, G. Dresselhaus, R. Saito, A. Jorio, *Phys. Rep.* **2005**, *409*, 47.
[37] M. S. Dresselhaus, A. Jorio, M. Hofmann, G. Dresselhaus, R. Saito, *Nano Lett.* **2010**, *10*, 751.
[38] A. C. Ferrari, J. C. Meyer, V. Scardaci, C. Casiraghi, M. Lazzeri, F. Mauri, S. Piscanec, D. Jiang, K. S. Novoselov, S. Roth, A. K. Geim, *Phys. Rev.* **2006**, *97*, 187401.

[39] R. Wang, Y. Hao, Z. Wang, H. Gong, J. T. L. Thong, *Nano Lett.* **2010**, *10*, 4844.
[40] D. J. Sellmyer, M. Zheng, R. Skomski, *Condens. Matter* **2001**, *13*, R433.
[41] J. Qin, J. Nogués, M. Mikhaylova, A. Roig, J. S. Munoz, M. Muhammed, *Chem. Mat.* **2005**, *17*, 1829.
[42] M. Grimsditch, Y. Jaccard, I. K. Schuller, *Phy. Rev. B* **1998**, *58*, 11539.
[43] G. C. Han, B. Y. Zong, P. Luo, Y. H. Wu, *J. Appl. Phys.* **2003**, *93*, 9202.
[44] J. Rivas, A. K. M. Bantu, G. Zaragoza, M. C. Blanco, M. A. López-Quintela, *J. Magn. Magn. Mater.* **2002**, *249*, 220.
[45] M. Vázquez, L. G. Vivas, *Phys. Status Solidi B* **2011**, *248*, 2368.
[46] M. Vázquez, K. Nielsch, P. Vargas, J. Velázquez, D. Navas, K. Pirota, M. Hernández-Vélez, E. Vogel, J. Cartes, R. B. Wehrspohn, U. Gosele, *Physica B* **2004**, *343*, 395.
[47] H. Cao, G. Huang, S. Xuan, Q. Wu, F. Gu, C. Li, *J. Alloys Compd.* **2008**, *448*, 272.
[48] F. Zighem, T. Maurer, F. Ott, G. Chaboussant, *J. Appl. Phys.* **2011**, *109*, 013910.
[49] T. Maurer, F. Zighem, W. Q. Fang, F. Ott, G. Chaboussant, Y. Soumare, K. A. Atmane, J. Y. Piquemal, G. Viau, *J. Appl. Phys.* **2011**, *110*, 123924.
[50] B. E. Kratochvil, M. Kumer, S. Erni, R. Borer, D. R. Frutiger, S. Schuerle, B. J. Nelson, *Proceedings of the12th International Symposium on Experimental Robotics*, New Delhi, India **2010**.
[51] S. Yasuda, D. N. Futaba, T. Yamada, J. Satou, A. Shibuya, H. Takai, K. Arakawa, M. Yumura, K. Hata, *ACS Nano* **2009**, *3*, 4164.
[52] D. Magnin, V. Callegari, S. Mátéfi-Tempfli, M. Mátéfi-Tempfli, K. Glinel, A. M. Jonas, S. Demoustier-Champagne, *Biomacromolecules* **2008**, *9*, 2517.
[53] A. Ahmad, K. Tetiana, K. Kern, K. Balasubramanian, *Chem. Phys. Chem.* **2009**, *10*, 2251.